IEEE Photonics Journal
An IEEE Photonics Society Publication

Efficient Experimental Design of a Long-Range Gapped Surface Plasmon Polariton Waveguide for Plasmonic Modulation Applications

Volume 11, Number 1, February 2019

Dong Hun Lee
Myung-Hyun Lee

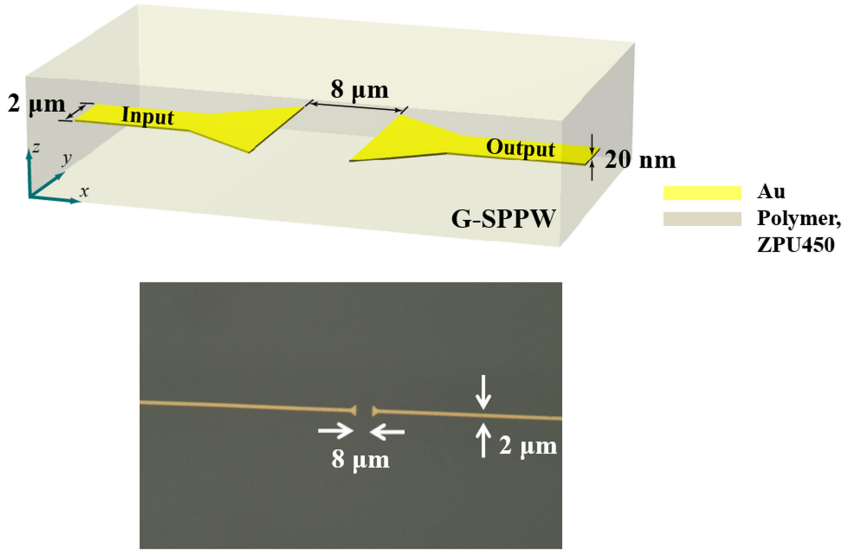

DOI: 10.1109/JPHOT.2019.2895093
1943-0655

Efficient Experimental Design of a Long-Range Gapped Surface Plasmon Polariton Waveguide for Plasmonic Modulation Applications

Dong Hun Lee and Myung-Hyun Lee

School of Electronic and Electrical Engineering, Sungkyunkwan University, Suwon 16419, South Korea

DOI:10.1109/JPHOT.2019.2895093

Manuscript received January 11, 2019; accepted January 21, 2019. Date of publication January 24, 2019; date of current version February 7, 2019. This work was supported by the National Research Foundation of Korea funded by the Korea government (MSIP) under Grant NRF-2017R1A2B2009128.
Corresponding author: Myung-Hyun Lee (e-mail: mhlee@skku.edu).

Abstract: We propose straight and tapered insulator–metal–insulator-type surface plasmon polariton (SPP) waveguides with a gap (G-SPPWs). The optical characteristics of the G-SPPWs are experimentally evaluated at a wavelength of 1.55 μm due to optical communication gateway. The parameters of the 20-nm-thick G-SPPWs were chosen based on our previous simulation results. The excited input SPPs propagate, jump over the gaps with low coupling losses, and propagate again, despite a 9-μm-long gap in the G-SPPWs. The coupling losses of the gap were experimentally determined to be less than 0.7 dB with various gap lengths up to 9 μm. The insertion losses of the straight G-SPPW with 8 μm $\times$ 2 μm (gap length $\times$ SPPW width) and the tapered G-SPPW with 8 μm $\times$ 2 μm (gap length $\times$ SPPW width) and a 6 μm $\times$ 3 μm (taper width $\times$ taper length) were determined to be $\sim$1.03 and $\sim$0.74 dB, respectively. The tapered structure increases the tunneling efficiency in the gap of the G-SPPW by reducing the insertion loss. In the 2.5-Gbps optical signal transmission experiment, the proposed G-SPPW exhibited excellent eye opening and transferred the carrier wave as well as the data signal. This device has potential as a new plasmonic modulation element offering control of a guided SPP through interaction with an applied force in the gap.

Index Terms: Surface plasmon polaritons (SPPs), Plasmonics, Waveguides, Integrated optics devices.

1. Introduction

The lowest dimension of optical elements is fundamentally determined by the diffraction limit of the light used, which is approximately half of the light wavelength. However, surface plasmon polaritons (SPPs) can overcome the diffraction limit of light [1]. SPPs are a high density electromagnetic wave, which arise from the interaction between the evanescent electromagnetic fields and the longitudinal collective oscillations of the free electrons in the metal-dielectric interfaces [2]. The SPP field components decay exponentially with an increasing distance in the metal-dielectric interfaces [3]. The SPPs have inherently large propagation losses because of internal damping in metal [4]. Therefore, SPPs are considered to be somewhat limited in application [5].

In a metal strip surrounded in a dielectric, SPPs are excited on top and bottom sides independently. However, in a sufficiently thin metal strip, the SPPs on each metal-dielectric interface couple and form a symmetric mode, which is a long-range SPP (LR-SPP) with respect to the orientation of the main electric field component [5], [6]. The thin metal strip embedded in a dielectric material with a finite width can be used as a LR-SPP waveguide (LR-SPPW). By controlling the width and thickness of the metal strip, and the refractive index of the surrounding dielectric material, the optical characteristics of the LR-SPPW can be properly adjusted [7]. For these reasons, the study of the LR-SPPW has been demonstrated in several integrated optical elements [8], [9]. Integrated optical devices based on LR-SPPWs have also been demonstrated, such as couplers, modulators, switches, and attenuators [10]–[12].

In general, it is not easy to control or modulate the guided LR-SPP in the insulator-metal-insulator waveguide (IMI-W) because of the straightness of SPPs at a wavelength of optical communication and a complex structure required for control and modulation of the guided LR-SPP [13]–[15]. For easy control and modulation of the guided LR-SPP, we proposed a straight IMI-type SPP waveguide with a gap (straight G-SPPW) and performed simulations [16], [17]. The two metal strips surrounded by a dielectric material are located longitudinally with a gap of a few μm. In addition, we proposed a tapered IMI-type SPP waveguide with a gap (tapered G-SPPW) and performed a simulation for the improvement of coupling efficiency in the gap [18], by adopting the linearly tapered LR-SPPWs [19]. Subsequently, Liu et al showed the characteristics of the straight G-SPPWs with simulation and experiment and successfully applied them to an in-line Mach-Zehnder interferometer thermal switch [20].

Various devices that use the interaction of a SPP and an applied force have been proposed for modulation of the guided SPP via electro-optic effects [21]–[23]. However, the proposed G-SPPWs can control or modulate a guided LR-SPP mode through direct interaction with an applied electric force in the gap of the G-SPPWs [17]. Also, to embody nano plasmonic integrated circuits (NPICs) that overcome the diffraction limit of light, waveguide-type plasmonic mode-size converters from microscale to nanoscale sizes are required. These have been partially realized with microscale LR-SPP modes successfully squeezed into nanoscale SPP modes via mode conversion in a SPPW-type device [24], [25]. The combination of the waveguide-type plasmonic mode-size converter and the G-SPPWs expedites the nano-sized plasmon-based circuits.

We experimentally investigated the optical characteristics of the G-SPPWs in LR-SPPWs, at a wavelength of 1.55 μm. This work represents an important step toward realization of a new plasmonic modulation device (PMD) with a simple structure for the control of guided LR-SPPs. We have already simulated and analyzed the straight G-SPPWs [16], [17] using finite-difference time-domain (FDTD) calculations. Also, to increase the tunnelling efficiency in the G-SPPWs, we have also simulated and analyzed the tapered G-SPPWs [18]. The optical characteristics of the fabricated straight and tapered G-SPPWs were measured and compared with simulation results. In addition, we performed a 2.5-Gbps optical signal transmission experiment of the proposed G-SPPWs to confirm the transfer of the data signal as well as the carrier wave for various PMD applications.

2. Design and Fabrication

2.1 Design of G-SPPWs

The simulated straight G-SPPW is composed of an input IMI-W 5 μm long and an output IMI-W 15 μm long, as shown in Fig. 1(a). The width and thickness of these IMI-Ws were fixed at 2 μm and 20 nm, respectively, through the simulation results [16]. We also adopted a design parameter of the different lengths (d_c) of the gap in the straight G-SPPWs, considering the simulation results [16]. Gold was used as a metal strip material, and a low-loss polymer was used as a dielectric for the 50-μm-thick upper and lower cladding layers. The refractive indices of the evaporated gold and the low-loss polymer were 0.550-11.4912i and 1.450, respectively, at a wavelength of 1.55 μm [7]. For practical applications, we limited the d_c in the straight G-SPPWs to maxima of $\sim$9 μm. Figure 1(b)

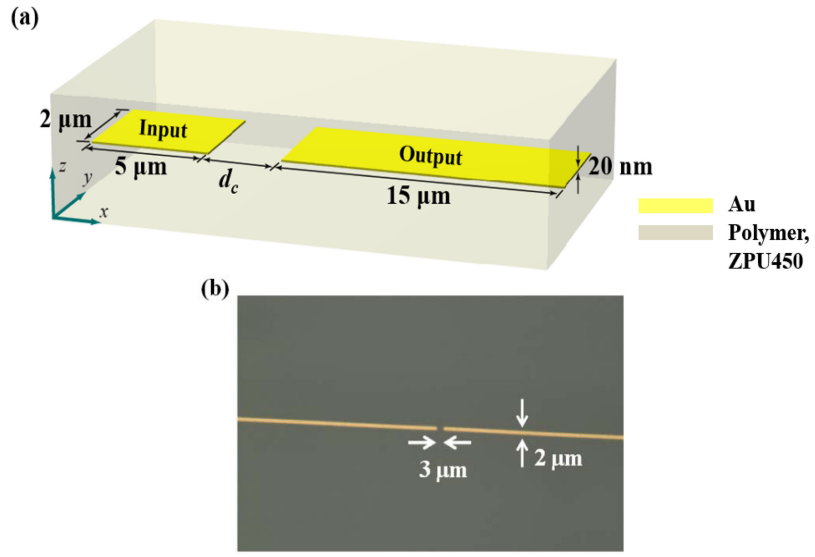

Fig. 1. (a) Schematic view of a straight G-SPPW. (b) Optical microscope image of the fabricated 2-μm-wide straight G-SPPW with a d_c of 3 μm.

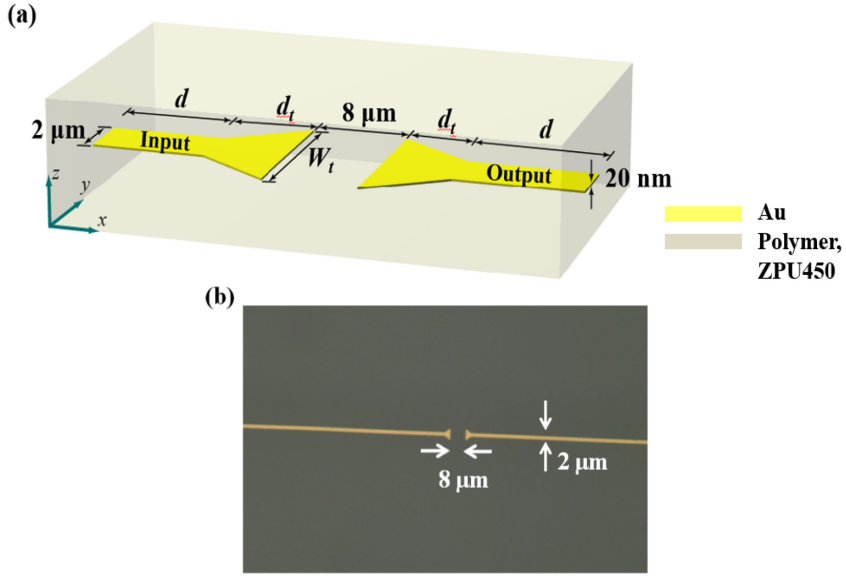

Fig. 2. (a) Schematic view of a tapered G-SPPW. (b) Optical microscope image of the fabricated tapered G-SPPW with a SPPW width of 2 μm, a d_c of 8 μm, a W_t of 4 μm, and a d_t of 3 μm.

shows an optical microscope image of the fabricated straight G-SPPW with a fixed SPPW width of 2 μm and a d_c of 3 μm.

Figure 2(a) shows a schematic view of the 28-μm-long tapered G-SPPW. This simulated device is composed of a reverse tapered input IMI-W 10 μm long ($d + d_t$) and a tapered output IMI-W 10 μm long ($d_t + d$) with an 8-μm-long gap by the simulation results. The width and thickness of the input and output SPPWs were also fixed at 2 μm and 20 nm, respectively, through the simulation results [16], [18]. We set various design parameters for the tapered G-SPPWs. These include variation in the widths (W_t) and lengths (d_t) of the tapered structure considering the simulation results [18].

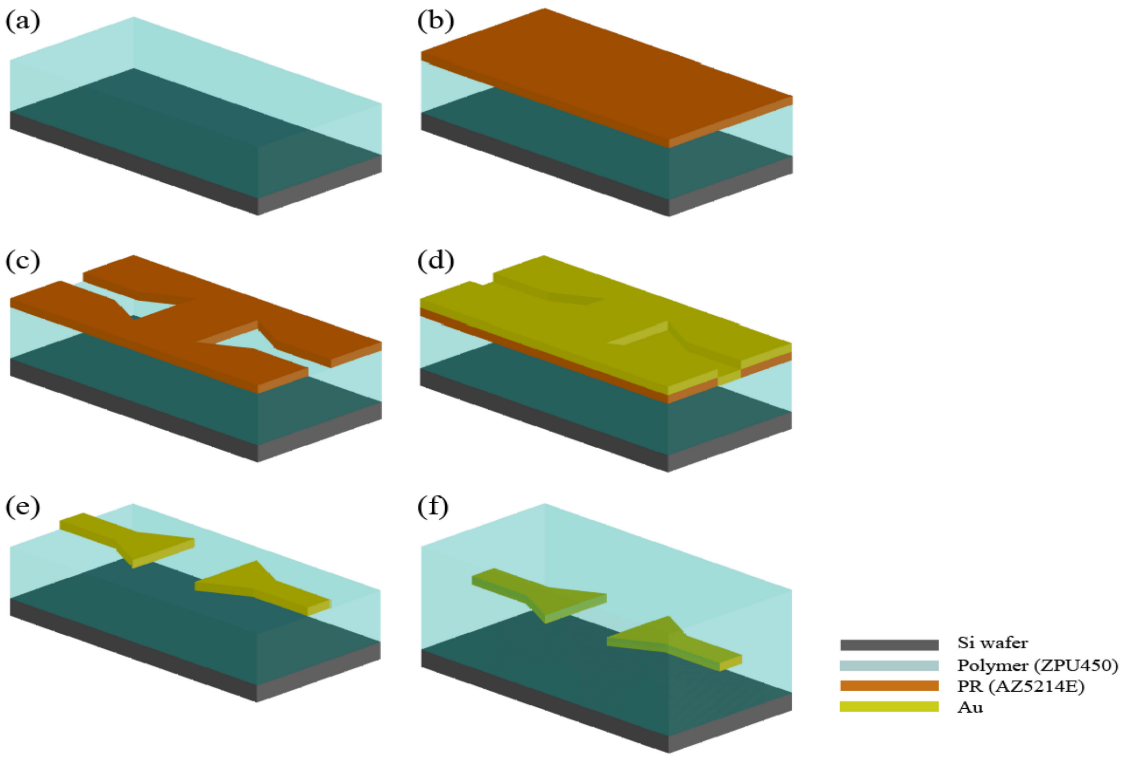

Fig. 3. Fabrication process of the G-SPPWs.

The proposed tapered structure can increase the tunnelling efficiency by reducing the insertion loss considering the coupling and propagation loss of the G-SPPWs. For practical applications, we limited W_t and d_t to $\sim 8\,\mu$m, respectively. Figure 2(b) shows an optical microscope image of the fabricated tapered G-SPPW with a SPPW width of 2 μm, a d_c of 8 μm, a W_t of 4 μm, and a d_t of 3 μm. For convenience of measurement, we fabricated the straight and tapered G-SPPW samples with total lengths of 1, 1.5, and 2 cm by increasing total lengths of the input and output SPPWs.

2.2 Fabrication of G-SPPWs

The gold strip is surrounded by a polymer in the G-SPPWs, as shown in Figs. 1 and 2; specifically, the polymer is an ultraviolet (UV)-curable epoxy, ZPU450, supplied by Chemoptics Inc., Korea. For convenience of explanation, we divide the polymer into upper and lower cladding layers of the same material. The propagation loss of the polymer is $\sim$0.3 dB/cm, and its refractive index is 1.45 [7]. For fabrication of samples, ZPU450 of 50 μm thickness was spin-coated on a 4-inch Si-wafer and then cured with UV light (365 nm) for 6 min at an optical power density of 20 mW/cm^2 in a nitrogen atmosphere as shown in Fig. 3(a). To obtain G-SPPWs of various parameters, the wafer was spin-coated with image reversal photoresist (PR, AZ5214E), exposed in contact photolithography, and developed in AZ500MIF as shown in Fig. 3(b), (c). Gold strips with 20 nm thickness were thermally evaporated followed by lift-off as shown in Fig. 3(d), (e). Onto that, ZPU450 was again spin-coated and cured with UV light to form an upper cladding layer of 50 μm thickness as shown in Fig. 3(f). The samples were cured at 200 °C for 30 min in a nitrogen oven (flow rate 50 L/min) to ensure the best curing and stability of the polymer layers. For the 2.5-Gbps optical signal transmission experiment, 1-cm-long samples of the fabricated straight and tapered G-SPPWs were prepared via dicing, and the end faces of the diced samples were polished and then pigtailed with polarization-maintaining single-mode fibers (PMSMFs).

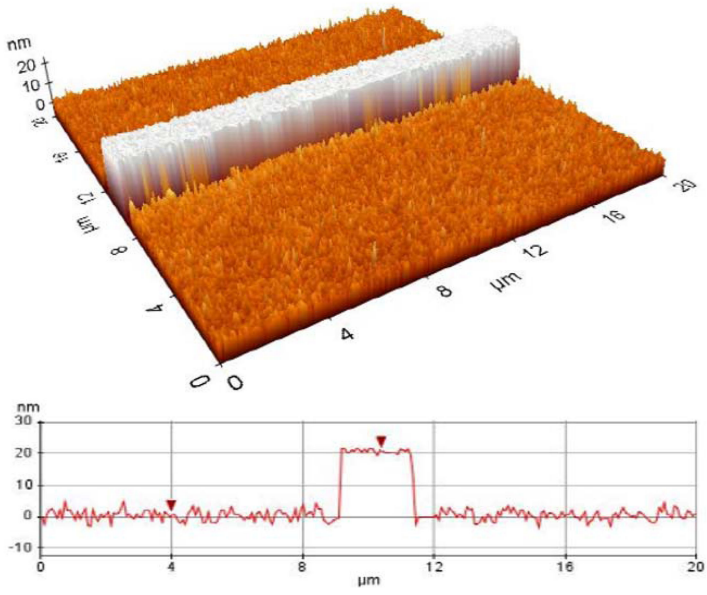

Fig. 4. AFM image of the evaporated 2-μm-wide Au strip with the 20 nm thickness on the 50-μm-thick low-loss polymer.

3. Results and Discussion

3.1 Experimental Results of Straight G-SPPWs

The physical characteristics of the fabricated 2-μm-wide G-SPPWs were analyzed via atomic force microscope (AFM), as shown in Fig. 4. As mentioned before, prior to the evaporation of the gold strips for input and output SPPWs in the G-SPPWs, the 50-μm-thick low-loss polymer was spin-coated and then cured on a 4-inch Si-wafer as a lower cladding layer. Therefore, the thickness of the gold strips was measured on the 50-μm-thick lower cladding layer via AFM and confirmed to be $\sim$20 nm, as shown in Fig. 4. A surface roughness less than 2 nm rms was also obtained by the AFM.

To examine the optical characteristics of the G-SPPWs, we used a measuring system consisting of an optical source of wavelength 1.55 μm, a polarization controller, and a power meter. Two PMSMFs were used to couple in and out at the input and output facets of the G-SPPW chip. To excite the input LR-SPP mode, the incident light from the optical source was transverse magnetic (TM) polarized with the polarization controller. The insertion loss in the straight G-SPPW is composed of propagation losses occurring in the SPPW and the gap, coupling losses occurring between the PMSMFs and the input and output facets of the G-SPPW chip, and coupling losses occurring at the rear of the input SPPW and the front of the output SPPW in the gap. Here, the propagation loss of the polymer in the gap is neglected because it is much less than that of the 20-nm-thick SPPW. The propagation and coupling losses between the PMSMFs and the input and output facets of the 20-nm-thick SPPW chip with SPPWs of lengths 1, 1.5, and 2 cm were measured and analyzed using a cut-back method [26].

Figure 5 shows experimental results of the coupling loss of the gap and the insertion loss of the 2-μm-wide straight G-SPPWs as a function of d_c. We already confirmed through simulations that a propagated SPP in the input SPPW excites a lightwave at the interface between the input SPPW and the gap, the excited lightwave propagates freely in the gap, the propagated lightwave again excites an SPP in the output SPPW, and the SPP propagates through the output SPPW [16]–[18]. Therefore, the coupling loss of the gap arises when the SPP jumps over the gap from the rear of the input SPPW to the front of the output SPPW in the G-SPPWs, as shown in Fig. 5. This loss was calculated by subtracting the propagation loss of the 2-μm-wide SPPW from the insertion loss

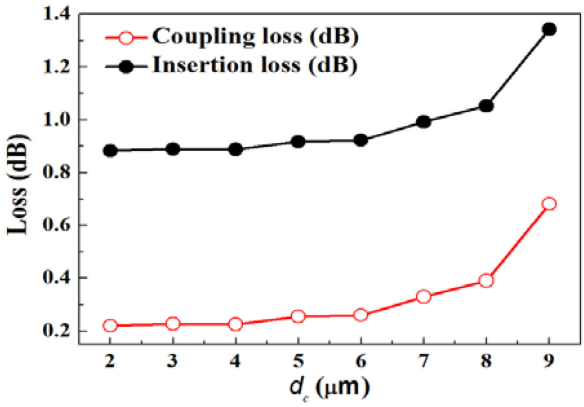

Fig. 5. Experimental results showing coupling loss of the gap and insertion loss of the 2-μm-wide straight G-SPPWs versus d_c.

of the straight G-SPPWs with various d_c. As mentioned before, we neglected the propagation loss of the polymer in the gap because it was calculated to be ~0.3 dB/cm, much lower than the ~8.73 dB/cm propagation loss of the 2-μm-wide SPPW [7]. The coupling losses of the gap with d_c less than 8 μm were less than ~0.38 dB. In contrast, when d_c is greater than 8 μm, those increase sharply with increasing d_c because of the mismatch of the mode field size between the free light wave in the gap and the SPP at the interface between the gap and the output SPPW. The minimum coupling loss of the gap was found to be ~0.22 dB with a d_c of 2 μm. The insertion losses include the propagation loss of the 2-μm-wide and 20-μm-long straight SPPW, the coupling loss of the gap with d_c up to ~9 μm, and the coupling loss of ~0.65 dB between the PMSMFs and the input and output straight G-SPPWs, as shown in Fig. 5. Here, the coupling loss of ~0.65 dB between the PMSMF and the input/output G-SPPW was estimated by linearly extrapolating the measured insertion losses from the 1-, 1.5-, and 2-cm-long SPPWs reference samples using the cut-back method [26]. The insertion losses of the straight G-SPPWs with d_c less than 8 μm were less than ~1.03 dB, whereas those with d_c greater than 8 μm increase sharply, as shown in Fig. 5. The trend observed in the insertion loss curve was similar to that of the coupling loss curve of the gap, as shown in Fig. 5. This occurred because the coupling losses of the gap with d_c up to ~9 μm were significantly greater than the propagation losses of the 2-μm-wide and 20-μm-long SPPW. Therefore, the insertion loss of the straight G-SPPWs is primarily determined by the coupling losses of the gap. The minimum insertion loss of ~0.88 dB among the straight G-SPPWs was obtained at a d_c of 2 μm. The d_c with the low coupling loss can be filled the variety of materials in the gap, such as nonlinear optical (NLO) materials, electro-optical (EO) materials, polarization controlled materials, and photo chromic materials. The guided SPP can be controlled optically or electrically by filling the gap with NLO/photochromic or EO materials. In principle, the SPP is excited and guided with a TM mode. The guided SPP can also be controlled by polarization via filling with polarization-controlled materials, such as a liquid crystal [17].

3.2 Experimental Results of Tapered G-SPPWs

The propagation loss of the G-SPPWs increases with increasing the width and thickness of the input/output LR-SPPWs [7]. However, the coupling loss of the gap in the G-SPPWs decreases with the same parameters. Therefore, the insertion loss of the G-SPPWs including the propagation loss and the coupling loss of the gap is affected by the width and thickness of the input/output LR-SPPWs. According to the simulation results based on a FDTD method, the maximum normalized transmission (NT) of -0.041 dB was obtained in the straight G-SPPW with a SPPW width of 2 μm, a SPPW thickness of 20 nm, and a d_c of 2 μm [16]. In the present work, the NT was inversely

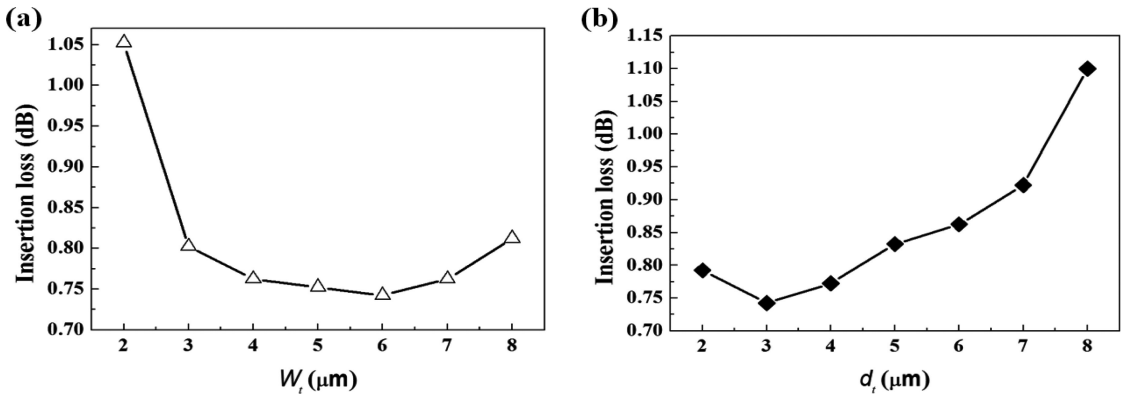

Fig. 6. Experimental results of insertion losses of the tapered G-SPPWs (a) with a fixed d_t of 3 μm versus W_t and (b) with a fixed W_t of 6 μm versus d_t.

proportional to the insertion loss of the straight G-SPPWs. Therefore, the SPP width of 2 μm and the SPP thickness of 20 nm were determined as the fixed width and thickness of the input/output SPPWs in the tapered G-SPPWs, as shown in Fig. 2(a). Also, as d_c increases, the coupling loss of the gap gradually increases up to d_c of 8 μm, and rapidly increase in the straight G-SPPWs with a fixed SPP width of 2 μm and a fixed SPPW thickness of 20 nm in the simulation results [16]. Therefore, the d_c of 8 μm was determined as a fixed length of the gap in the tapered G-SPPWs considering an inflection point (at the 8 μm-long d_c) of the coupling loss of the gap in the straight G-SPPW, as shown in Fig. 2(a). We limited the length of the tapered structure up to d_t of $\sim$8 μm. Because the length of the input and output SPPWs in the tapered G-SPPWs set 10 μm, respectively, in the simulation [18]. The simulated tapered G-SPPWs were obtained with the insertion loss less than the straight G-SPPWs by using the tapered structure. The tapered structure decreases the insertion loss through pseudo-adiabatic mode-size conversion with a small radiation loss in the tapered G-SPPWs. According to these simulation results, the straight and tapered G-SPPWs were compared with a fixed SPPW width of 2 μm, a fixed SPPW thickness of 20 nm, and a fixed d_c of 8 μm for verification of the simulation results through the measurement results of the fabricated G-SPPWs.

Figure 6(a) shows the experimental results of the insertion loss of the 28-μm-long tapered G-SPPWs with a fixed d_t of 3 μm as a function of W_t. As W_t increases, the insertion loss of the tapered G-SPPW decreases sharply up to W_t of 3 μm and then decreases gradually up to W_t of 6 μm. Subsequently, the insertion loss of the tapered G-SPPWs increases gradually up to W_t of 8 μm. The minimum insertion loss of the tapered G-SPPWs was found to be $\sim$0.74 dB for a W_t of 6 μm. The insertion loss of the 28-μm-long tapered G-SPPWs includes the propagation losses of the 2-μm-wide input and output SPPW, the loss of the tapered region, and the coupling loss between the PMSMFs and the input and output tapered G-SPPWs, as shown in Fig. 6. Herein, the loss of the tapered region is defined as the propagation loss + the mode conversion loss + the coupling loss of the gap in the tapered structure. The loss of the tapered region with W_t up to 8 μm and d_t up to 8 μm, respectively, was less than 0.39 dB. By the tapered structure, the insertion loss of the tapered G-SPPWs has a gain of more than 0.14 dB compared to the straight G-SPPWs. Figure 6(b) shows the experimental results of the insertion loss of the 28-μm-long tapered G-SPPWs with a fixed W_t of 6 μm as a function of d_t. The fixed d_t of 3 μm and W_t of 6 μm parameters were adopted based on simulation results [18], as shown in Fig. 6 because the maximum NT of $-$0.042 dB was obtained for the tapered G-SPPW with the d_t of 3 μm and the W_t of 6 μm via the FDTD method. As d_t increases, the insertion loss of the tapered G-SPPW decreases gradually up to d_t of 3 μm and then increases up to d_t of 8 μm, as shown in Fig. 6(b).

The minimum insertion loss of $\sim$0.74 dB among the tapered G-SPPWs with a fixed W_t of 6 μm was obtained at a d_t of 3 μm. These results show an optimized tapered region with the 6-μm-wide

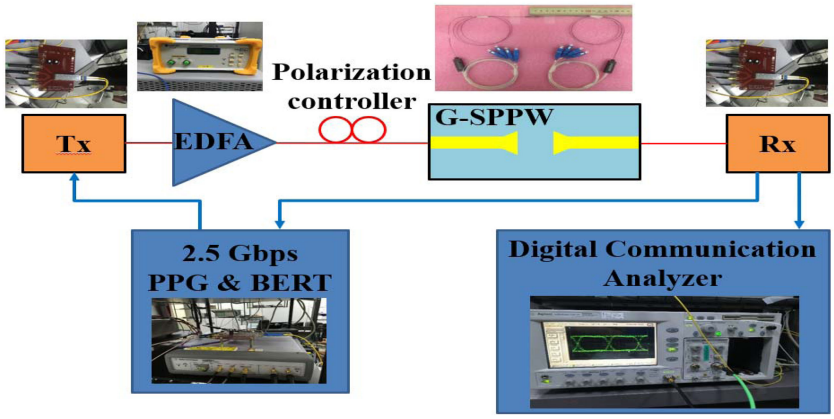

Fig. 7. Experimental setup for a 2.5-Gbps optical signal transmission. The insets show measuring equipment for a 2.5-Gbps optical signal transmission and a 4 channel-pigtailed G-SPPW chip.

taper width (W_t) and the 3-μm-long taper length (d_t) in the tapered G-SPPWs. Thus, there is a clear correlation between the W_t and d_t to obtain maximum tunnelling efficiency in the gap. Also, when comparing the experimental results of the 20-nm-thick straight and tapered G-SPPWs, the insertion losses of the straight G-SPPW with a d_c of 8 μm and a SPPW width of 2 μm and the tapered G-SPPW with a d_c of 8 μm, a SPPW width of 2 μm, a W_t of 6 μm, and a d_t of 3 μm were determined to be $\sim$1.03 and $\sim$0.74 dB, respectively. These experimental results mean that the proposed tapered region decreases the insertion loss considering the coupling and propagation loss of the G-SPPWs for improving the efficiency of the tunnelling. In general, a NPIC for high-speed and high-signal processing are required with high-integration and low-power consumption. They are integrated into a number of nano optical devices with low-power consumption. Therefore, the little difference between the insertion loss of the straight G-SPPWs and the tapered G-SPPWs results in a huge low-power consumption in the NPIC where a number of nano optical devices are integrated.

3.3 Data Transmission Experiment of G-SPPWs

So far it has been demonstrated that SPPs in the G-SPPWs are transmitted as a carrier wave. However, for data signal transfer, experiments on 10 and 40 Gbps signal transmissions with SPPWs have been conducted, showing excellent results [6], [7]. We performed a 2.5-Gbps optical signal transmission experiment with the proposed SPPWs with a gap (G-SPPWs), at the wavelength of 1.55 μm.

The experimental setup is shown in Fig. 7. An Agilent technologies Inc. N5980A 2.5-Gbps pulse pattern generator (PPG, data rate: 2,488.32 Mb/s, data pattern: $2^{23}-1$), an Agilent technologies Inc. N5980A bit error rate tester (BERT), a LUXPERT Inc. LXI-2000 erbium-doped fiber amplifier (EDFA), and an Agilent technologies Inc. 86100B digital communication analyzer (DCA) were used. A polarization controller was also used because the LR-SPP is excited by TM mode light. Finally, a Lightron Inc. SFP48-US3LC-KTA 1.55 μm laser diode was used for the carrier wave.

Figure 8 shows the measured eye diagrams for the 1-cm-long tapered G-SPPW with a W_t of 4 μm and a d_t of 3 μm under a 2.5-Gbps optical signal transmissions, including a back-to-back eye diagram and an eye diagram after transmission. In the eye diagram after transmission, the input signal was amplified to a power level of 10 dBm using the EDFA, and then the signal was passed through the polarization controller to excite the TM mode light. The eye pattern of the propagated signal from the G-SPPW was measured with the DCA. The parameters of scale and time for measured eye diagrams in the DCA were fixed at 55.1 mV/div and 100 ps/div, respectively. As shown in Fig. 8(b), the eye was well open, even though there were many obstacles such as the gap of the G-SPPWs,

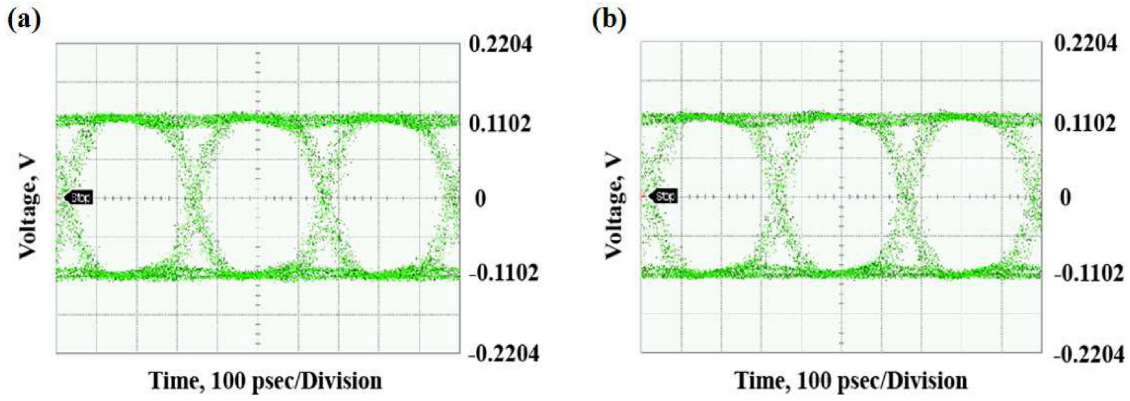

Fig. 8. Measured eye diagrams of an 1-cm-long tapered G-SPPW with a W_t of 4 μm and a d_t of 3 μm under a 2.5-Gbps optical signal transmission: (a) back-to-back and (b) after transmission.

longitudinal oscillations of the electrons, propagation loss, wave vector difference, and dispersion. Thus, we confirmed that the proposed G-SPPWs transmitted the data signal as well as the carrier wave. These results indicate that the G-SPPW has potential applicability for new PMD applications via control of the guided SPP through interaction with an applied force in the gap.

4. Conclusion

We confirm experimentally that SPPs propagate, jump over a gap, and propagate again in straight and tapered G-SPPWs. The SPP propagates through the input and output SPPWs even though there is a long gap of 9 μm in the G-SPPW. The coupling loss of the gap sharply increased at 9-μm-long gap. The insertion losses of the straight G-SPPW with 8 μm gap length and 2 μm SPPW width and the tapered G-SPPW with 8 μm gap length, 2 μm SPPW width, 6 μm taper width, and 3 μm taper length were determined to be $\sim$1.03 and $\sim$0.74 dB, respectively. The tapered G-SPPWs with 8 μm gap length and 2 μm SPPW width improve the efficiency of the tunnelling by reducing the insertion loss considering the coupling and propagation loss of the G-SPPWs. We also demonstrated that the proposed G-SPPWs transferred the data signal as well as the carrier wave in the 2.5-Gbps optical signal transmission experiment. The G-SPPW has potential as a new plasmonic modulation element, offering control of the guided SPP through interaction with an applied force in the gap.

References

[1] W. L. Barnes, A Dereux, and T. W. Ebbesen, "Surface plasmon subwavelength optics," *Nature*, vol. 424, no. 6950, pp. 824–830, 2003.
[2] H. Raether, *Surface Plasmons on Smooth and Rough Surfaces and on Gratings*. Berlin, Germany: Springer, 1988, ch. 2, pp. 4–37.
[3] G. Nemova and R. Kashyap, "Theoretical model of a planar integrated refractive index sensor based on surface plasmon-polariton excitation," *Opt. Commun.*, vol. 275, no. 1, pp. 76–82, 2007.
[4] T. Nikolajsen, K. Leosson, I. Salakhutdinov, and S. I. Bozhevolnyi, "Polymer-based surface-plasmon-polariton stripe waveguides at telecommunication wavelengths," *Appl. Phys. Lett.*, vol. 82, no. 5, pp. 668–670, 2003.
[5] A. Boltasseva, T. Nikolajsen, K. Leosson, K. Kjaer, M. S. Larsen, and S. I. Bozhevolnyi, "Integrated optical components utilizing long-range surface plasmon polaritons," *J. Lightw. Technol.*, vol. 23, no. 1, pp. 413–422, Jan. 2005.
[6] J. J. Ju *et al.*, "40 Gbit/s light signal transmission in long-range surface plasmon waveguides," *Appl. Phys. Lett.*, vol. 91, no. 17, 2007, Art. no. 171117.
[7] J. J. Ju *et al.*, "Polymer-based long-range surface plasmon polariton waveguides for 10-Gbps optical signal transmission applications," *J. Lightw. Technol.*, vol. 26, no. 11, pp. 1510–1518, Jun. 2008.
[8] R. Charbonneau, N. Lahoud, G. Mattiussi, and P. Berini, "Demonstration of integrated optics elements based on long-ranging surface plasmon polaritons," *Opt. Exp.*, vol. 13, no. 3, pp. 977–984, 2005.

[9] R. Charbonneau *et al.*, "Passive integrated optics elements based on long-range surface plasmon polaritons," *J. Lightw. Technol.*, vol. 24, no. 1, pp. 477–494, Jan. 2006.
[10] H. S. Won *et al.*, "Vertical coupling of long-range surface plasmon polaritons," *Appl. Phys. Lett.*, vol. 88, no. 1, 2006, Art. no. 011110.
[11] T. Nikolajsen, K. Leosson, and S. I. Bozhevolnyi, "Surface plasmon polariton based modulators and switches operating at telecom wavelengths," *Appl. Phys. Lett.*, vol. 85, no. 24, 2004, Art. no. 5833.
[12] B. Alam, A. Veroli, and A. Benedetti, "Analysis on vertical directional couplers with long range surface plasmons for multilayer optical routing," *J. Appl. Phys.*, vol. 120, no. 8, 2016, Art. no. 083106.
[13] A. Melikyan *et al.*, "Surface plasmon polariton absorption modulator," *Opt. Exp.*, vol. 19, no. 9, pp. 8855–8869, 2011.
[14] A. Emboras *et al.*, "Electrically controlled plasmonic switches and modulators," *IEEE J. Sel. Topics Quantum Electron.*, vol. 21, no. 4, Jul./Aug. 2015, Art. no. 4600408.
[15] M. Ayata *et al.*, "High-speed plasmonic modulator in a single metal layer," *Science*, vol. 358, no. 6363, pp. 630–632, 2017.
[16] D. H. Lee and M.-H. Lee, "Gapped surface plasmon polariton waveguides for plasmonic signal modulation applications," *J. Nanosci. Nanotechnol.*, vol. 15, no. 10, pp. 7679–7684, 2015.
[17] D. H. Lee and M.-H. Lee, "Gapped surface plasmon polariton waveguide device based on a liquid crystal," *J. Nanosci. Nanotechnol.*, vol. 15, no. 10, pp. 7711–7716, 2015.
[18] D. H. Lee and M.-H. Lee, "Discontinuous tapered surface plasmon polariton waveguides with gap," *J. Nanosci. Nanotechnol.*, vol. 16, no. 6, pp. 6275–6280, 2016.
[19] W.-J. Lee *et al.*, "Enhanced transmission in a fiber-coupled Au stripe waveguide system," *IEEE Photon. Technol. Lett.*, vol. 22, no. 2, pp. 100–102, Jan. 2010.
[20] T. Liu *et al.*, "Transmission of long-range surface plasmon-polaritons across gap in Au waveguide," *J. Opt.*, vol. 18, no. 1, 2016, Art. no. 015006.
[21] M. J. Dicken, L. A. Sweatlock, D. Pacifici, H. J. Lezec, K. Bhattacharya, and H. A. Atwater, "Electrooptic modulation in thin film barium titanate plasmonic interferometers," *Nano Lett.*, vol. 8, no. 11, pp. 4048–4052, 2008.
[22] W. Cai, J. S. White, and M. L. Brongersma, "Compact, high-speed and power-efficient electrooptic plasmonic modulators," *Nano Lett.*, vol. 9, no. 12, pp. 4403–4411, 2009.
[23] N. Hojo *et al.*, "Analysis of plasmonic phase modulator with furan-thiophene chromatophore electro-optic polymer," *Appl. Opt.*, vol. 56, no. 8, pp. 2053–2059, 2017.
[24] H.-R. Park, J.-M. Park, M.-S. Kim, and M.-H. Lee, "A waveguide-typed plasmonic mode converter," *Opt. Exp.*, vol. 20, no. 17, pp. 18636–18645, 2012.
[25] H.-R. Park, D. H. Lee, J.-H. Son, M.-S. Kim, and M.-H. Lee, "Sa0 mode converter for nano plasmonic integrated circuits," *J. Nanosci. Nanotechnol.*, vol. 13, no. 9, pp. 6389–6394, 2013.
[26] Y. A. Vlasov and S. J. McNab, "Losses in single-mode silicon-on-insulator strip waveguides and bends," *Opt. Exp.*, vol. 12, no. 8, pp. 1622–1631, 2014.